AGU PUBLICATIONS

Radio Science

RESEARCH ARTICLE
10.1002/2015RS005719

Key Points:
- Scintillation at low latitudes is typically more severe than at high latitudes
- Scintillation events are generally more severe on L2 and L5 than on L1
- High-latitude scintillation is highly correlated with geomagnetic activity

Correspondence to:
Y. Jiao,
jiaoy2@rams.colostate.edu

Citation:
Jiao, Y., and Y. T. Morton (2015), Comparison of the effect of high-latitude and equatorial ionospheric scintillation on GPS signals during the maximum of solar cycle 24, *Radio Sci.*, *50*, 886–903, doi:10.1002/2015RS005719.

Received 28 MAR 2015
Accepted 20 AUG 2015
Accepted article online 25 AUG 2015
Published online 25 SEP 2015

Comparison of the effect of high-latitude and equatorial ionospheric scintillation on GPS signals during the maximum of solar cycle 24

Yu Jiao[1] and Yu T. Morton[1]

[1]Department of Electrical and Computer Engineering, Colorado State University, Fort Collins, Colorado, USA

Abstract Radio signal scintillation caused by electron density irregularities in the ionosphere affects the accuracy and integrity of Global Navigation Satellite Systems, especially in the equatorial and high-latitude regions during solar maxima. Scintillation in these two regions, nevertheless, is usually influenced by different factors and thus has different characteristics that cause different effects on GNSS signals. This paper compares the characteristics of high-latitude and equatorial scintillation using multifrequency GPS scintillation data collected at Gakona, Alaska, Jicamarca, Peru, and Ascension Island during the 24th solar maximum. Several statistical distributions are established based on the data to characterize the intensity, duration, and occurrence frequency of scintillation. Results show that scintillation in the equatorial region is generally more severe and longer lasting, while high-latitude scintillation is, in general, more moderate and usually dominated by phase fluctuations. Results also reveal the different impacts of solar activity, geomagnetic activity, and seasons on scintillation in different geographic locations.

1. Introduction

Ionospheric scintillation refers to the random amplitude and phase fluctuations observed in radio signals propagating through electron density irregularities in the ionospheric plasma and most commonly occurs in equatorial, auroral, and polar regions [*Yeh and Liu*, 1982; *Aarons*, 1982; *Aarons and Basu*, 1994; *Jiao et al.*, 2013c]. Occurrence of scintillation is difficult to predict and model due to the variability of its numerous influencing factors, which include solar activities, interplanetary magnetic field activities, local electric field, and conductivity, convection processes, and wave interactions [*Aarons*, 1982; *Tsunoda*, 1988; *Pi et al.*, 1997; *Basu et al.*, 2002; *Kintner et al.*, 2004; *Smith et al.*, 2008; *Redmon et al.*, 2010; *Liu et al.*, 2013]. Transionospheric radio waves, such as the Global Navigation Satellite System (GNSS) signals, are vulnerable to scintillation. Strong scintillation can severely impact the acquisition and tracking process in GNSS receivers, causing a degradation in navigation solution accuracy, integrity, and continuity [*Skone*, 2001; *Skone et al.*, 2001; *Kintner et al.*, 2007; *Seo et al.*, 2007; *Xu et al.*, 2012; *Carroll et al.*, 2014; *Fortes et al.*, 2014; *Morton et al.*, 2014; *Xu and Morton*, 2015]. As GNSS technology becomes a crucial component for a functional, technologically advanced society in such areas as intelligent transportation, precision agriculture, consumer electronics, and remote sensing, there is a great need that is to have a better understanding of the characteristics and impact of ionospheric scintillation affecting both scientific and engineering areas of interest.

It is often of interest to monitor and model ionospheric scintillation in two contrasting regions in the world: the equatorial region (within ±20° around the magnetic equator) and high-latitude regions including auroral and polar zones [*Aarons*, 1982; *Basu et al.*, 2002]. The former area is known to be plagued with frequent and strong scintillation, especially deep amplitude fading, after local sunset caused by the up-rising and disintegration of the Rayleigh-Taylor instability (bubbles) in the *F* region equatorial ionosphere [*Kelley et al.*, 1981; *Hysell et al.*, 1990; *Hysell and Kudeki*, 2004]. Research also shows that equatorial scintillation is more frequent and intense around equinoxes and subsides in the summer [*Aarons*, 1982; *Tsunoda*, 1985; *Kintner et al.*, 2007; *Beniguel et al.*, 2009]. In high-latitude regions, where irregularity patches are presumed to be caused by gradient drift instability and accelerated energetic electron precipitation along geomagnetic field lines, the observed ionospheric scintillation is greatly associated with solar transients and thus may become severe during disturbances in the geomagnetic field of the Earth [*Basu et al.*, 2002]. Positive correlation between high-latitude scintillation and global geomagnetic field activities has been observed using the global geomagnetic field activity indices *K*/*Kp*, *Ap*, and *Dst* [*Dagg*, 1957; *Das Gupta et al.*, 1985; *Basu et al.*, 2002; *Rodrigues et al.*, 2004;

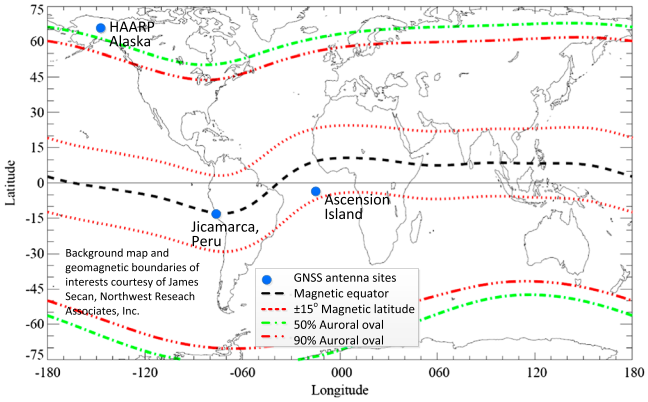

Figure 1. Global map showing the geographic locations of the three antenna sites represented in blue dots. The bands of the magnetic equatorial area and the auroral ovals are estimations.

Reggiani et al., 2005; *Hasbi et al.*, 2007; *Li et al.*, 2008; *Shang et al.*, 2008]. Studies have also revealed scintillation's close relationship with variations in local geomagnetic field components [*Prikryl et al.*, 2010, 2011; *Jiao et al.*, 2013b]. In addition, high-latitude scintillation is usually observed to be dominated by phase fluctuations at the L-band frequencies used by Global Positioning System (GPS) signals [*Buchau et al.*, 1984; *Valladares et al.*, 2002; *Kintner et al.*, 2007; *Skone et al.*, 2008; *Azeem et al.*, 2013]. Several previous research findings showed that auroral scintillation is usually a nighttime phenomenon, while polar cap scintillation exists at all local times [*Kintner et al.*, 2007; *Li et al.*, 2010; *Jiao et al.*, 2013a, 2013c]. Previous literature also showed that high-latitude scintillation has a location-dependent seasonal pattern of occurrence with more events reported during winter and equinox [*Rino et al.*, 1983; *Kersley et al.*, 1988, 1995; *Aquino et al.*, 2005; *Kintner et al.*, 2007; *De Franceschi et al.*, 2006; *Li et al.*, 2010; *Alfonsi et al.*, 2011; *Prikryl et al.*, 2011; *Jiao et al.*, 2013c].

The objective of this paper is to analyze and compare characteristics of ionospheric scintillation observed in equatorial and high-latitude regions, using the latest multifrequency GPS data collected during the 24th solar maximum. The GPS data were collected at three different locations: Gakona, Alaska (geographic: 62.4°N, 145.2°W; geomagnetic: 63.5°N, 92.2°W), Jicamarca, Peru (geographic: 11.9°S, 76.9°W; geomagnetic: 2.0°S, 4.3°W), and Ascension Island (geographic: 7.9°S, 14.4°W; geomagnetic: 2.6°S, 57.3°E). Their geographic locations are illustrated in Figure 1. Gakona is located in the northern auroral oval where the authors of this paper have been collecting GNSS data since 2010 [*Pelgrum et al.*, 2011; *Vikram*, 2011; *Taylor et al.*, 2012]. Jicamarca and Ascension Island are near the magnetic equator. A multi-GNSS data collection system has been collecting data at Jicamarca since November 2012, while a similar system was deployed on Ascension Island for an experimental campaign in March 2013. The analysis presented in this paper is based on data collected by a GPS Silicon Valley GSV4004B receiver (L1C/A signal) and a Septentrio PolaRxS receiver (L2C and L5 signals) at Gakona, and multiband data collected by Septentrio PolaRxS receivers at Jicamarca and Ascension Island.

A set of criteria have been established to filter scintillation events from the high-rate measurement data based on the values of the two commonly used scintillation indices: the amplitude scintillation indicator S_4, and the phase scintillation indicator σ_ϕ. The events extracted are then processed to obtain several important features of scintillation occurring in different regions considered in this paper. Results clearly show the characteristics and differences in scintillation intensity and duration across frequency bands, diurnal and seasonal dependencies, and also the correlation with geomagnetic activities that were observed at the three antenna sites. These results show agreement with earlier work in ionospheric scintillation and provide detailed numerical statements and comparisons, which will be helpful in the future study of the nature of ionosphere and scintillation, as well as in the development of robust scintillation mitigation receiver design.

The rest of the paper is organized as follows. Section 2 describes the data collection systems and the data set used in the analysis. Section 3 introduces the two scintillation indicators and the event filtering procedures. Section 4 characterizes scintillation results at different locations. Section 5 is a summary and recommendations for future work.

2. Data Collection Systems and Available Data Set

A high-latitude GNSS receiver setup was established in 2009 at Gakona, Alaska, which is located within the 50% auroral oval zone [*Taylor et al.*, 2012]. The setup evolved into an array of four antennas, each connected to a commercial ionospheric scintillation-monitoring (ISM) receiver (GSV4004B receiver or PolaRxS receiver in

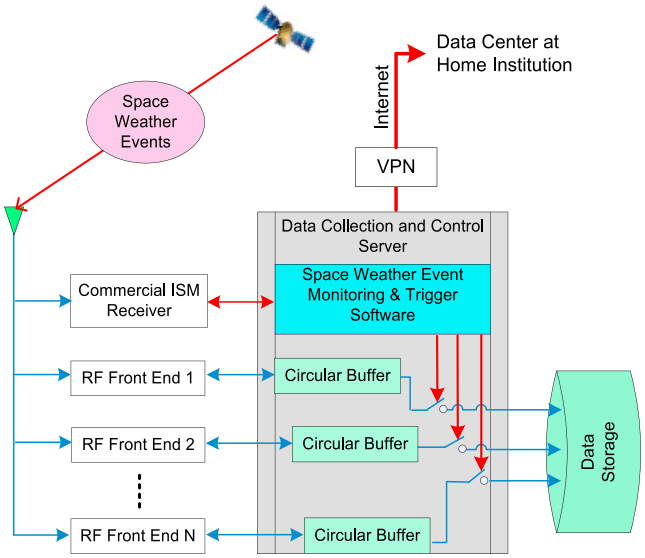

Figure 2. General architecture of the event-driven GNSS data collection systems deployed at several high-latitude and equatorial sites. The GSV4004B and the PolaRxS receivers are the commercial ISM receivers which are used to collect full-time navigation data and trigger the data collection of the RF front ends. All the data analyzed in this study are from the two ISM receivers.

this study) and several software defined radio (SDR) front-ends (Figure 2). The ISM receivers continuously collect measurement data including I and Q channel correlator outputs and carrier phase. Scintillation indices and scintillation event indicator are computed from the ISM measurements. The indicators are continuously compared with preset threshold values to trigger the data server to record raw intermediate frequency (IF) samples generated by the SDR front-ends [*Taylor et al.*, 2013; *Jiao et al.*, 2013c; *Xu and Morton*, 2015]. These event-driven SDR front-end recorded data are used for advanced scintillation receiver algorithm development and for postprocessing and analysis of strong scintillation signals.

In this study, only the ISM data are used to provide a general characterization of high-latitude and equatorial scintillation. High-latitude GPS L1C/A scintillation, as discussed in section 4, is based on 1038 days of GPS data collected by a GSV4004B receiver [*Van Dierendonck et al.*, 1993, 1996; *Van Dierendonck and Arbesser-Rastburg*, 2004] from August 2010 to June 2014. The GSV4004B outputs 50 Hz phase and amplitude measurements only for the GPS L1C/A signal. Table 1 lists monthly normal operation days, and the percentage of time when data were collected. The high-latitude scintillation data on L2C and L5 were collected by a Septentrio PolaRxS receiver from August 2012 to March 2013. The corresponding monthly sum of normal operation days and the percentage are listed in Table 2. Collocated at the GNSS receiver array site is a fluxgate geomagnetometer operated by the High Frequency Active Auroral Research Program (HAARP). The magnetometer recorded 1 Hz *H* (horizontal), *D* (declination), and *Z* (vertical) components of the local geomagnetic field until June 2013. The data were also available on the Alaska Satellite Facility website at https://www.asf.alaska.edu/magnetometer/ download.

The equatorial scintillation data studied in this paper were collected at two locations—Jicamarca, Peru, and Ascension Island, by the event-driven GNSS data collection system shown in Figure 2. The former site is

Table 1. Number and Percentage of Days of L1C/A Data Available From the GSV4004B Receiver at Gakona, Alaska

Year	2010		2011		2012		2013		2014	
Month	No. of Days	%	No. of Days	%	No. of Days	%	No. of Days	%	No. of Days	%
Jan	Not available		31	100	7.8	25.2	21.8	70.3	0	0
Feb			28	100	19.8	68.3	28	100	25	89.3
Mar			23	74.2	15.1	48.7	31	100	31	100
Apr			28.9	96.3	0	0	30	100	30	100
May			31	100	0	0	14	45.2	31	100
Jun			30	100	22.3	74,3	30	100	22	73.3
Jul			17	54.8	28	90.3	31	100	Not available	
Aug	6	19.4	21	67.7	26.8	86.5	31	100		
Sep	28	90.3	0	0	30	100	30	100		
Oct	15	48.4	6	19.4	31	100	31	100		
Nov	29	96.7	14	46.7	30	100	24.9	83.0		
Dec	31	100	18.6	60	8	25.8	19.8	63.9		
Total	109	71.2	248.6	68.1	218.8	59.8	322.5	88.4	139	76.8
			Grand total in 2010–2014						1037.9	72.6

Table 2. Number and Percentage of Days of L2C and L5 Data Available From the Septentrio PolaRxS Receiver at Gakona, Alaska

Year	2012		2013	
Month	No. of Days	%	No. of Days	%
Jan	Not available		24.2	78.2
Feb			6.1	21.7
Mar			29.7	95.7
Apr			Not available	
May				
Jun				
Jul				
Aug	26.3	84.9		
Sep	28.1	93.6		
Oct	31	100		
Nov	30	100		
Dec	31	100		
Total	146.4	95.7	60.0	66.7
Grand total in 2012 and 2013			206.4	85.0

located at Jicamarca Radio Observatory (JRO), close to the geomagnetic equator [*Jiao et al.*, 2014]. Only GPS data collected by the commercial ISM receiver, a Septentrio PolaRxS receiver, are used in this study. This receiver generates 100 Hz phase measurements and 100 Hz correlator outputs on all three GPS bands (L1C/A, L2C, and L5), which are further processed to generate 50 Hz signal intensity measurements. In addition, this receiver can also collect data from other GNSS constellations (GLONASS, Galileo, and BeiDou), although these data are not discussed in this study. Table 3 summarizes the number and percentage of days of data available from Jicamarca, Peru, from November 2012 to July 2014. Similar to HAARP, JRO also operates a geomagnetometer, which provides 1/60 Hz measurements of the *H*, *D*, *Z*, *I* (inclination), and *F* (intensity) local geomagnetic components.

The Ascension Island data were collected during a campaign from 1 to 10 March in 2013 using a setup similar to the one described in Figure 2. Only the Septentrio PolaRxS ISM receiver data were used in this study. The data were collected over a 10 day period during which a number of very strong scintillation events were captured. Unfortunately, no local geomagnetic data are available on Ascension Island for this period of time.

3. Scintillation Indices and Event Thresholds

The raw signal intensity and carrier phase measurements from the ISM receivers were detrended using a sixth-order Butterworth filter with a 0.1 Hz cutoff frequency [*Van Dierendonck et al.*, 1993]. The detrended

Table 3. Number and Percentage of Days of L1C/A, L2C and L5 Data Available From Jicamarca, Peru

Year	2012		2013		2014	
Month	No. of Days	%	No. of Days	%	No. of Days	%
Jan	Not available		29.5	95.1	0	0
Feb			28	100	6.9	24.7
Mar			30.0	96.8	24.0	77.4
Apr			28.5	94.9	24.1	80.4
May			22.5	72.7	0	0
Jun			12.6	42.0	0.1	0.4
Jul			0	0	29.7	95.7
Aug			5.3	17.0	Not available	
Sep			14.1	47.1		
Oct			26.6	85.6		
Nov	8	26.7	11.8	39.3		
Dec	31	100	0	0		
Total	39	63.9	208.9	57.2	84.8	40.0
Grand total in 2012–2014					332.7	52.1

measurements are then used to compute the two scintillation indices: S_4 and σ_ϕ based on equations (1) and (2). S_4 is a measurement of amplitude scintillation, which is defined as the standard deviation of the detrended received signal power normalized to the average signal power [*Briggs and Parkin*, 1963]. The phase fluctuation indicator σ_ϕ is defined as the standard deviation of the detrended signal carrier phase measurements [*Yeh and Liu*, 1982].

$$S_4 = \sqrt{\frac{\langle I^2 \rangle - \langle I \rangle^2}{\langle I \rangle^2}} \tag{1}$$

$$\sigma_\phi = \sqrt{\langle \phi^2 \rangle - \langle \phi \rangle^2} \tag{2}$$

In the two equations, I and ϕ stand for detrended signal intensity and carrier phase, respectively, and $<\cdot>$ represents the expected value over the interval of interest. In this study, the interval of interest was set to 10 s to most effectively highlight scintillation features based on evaluations of several different time intervals between 10 and 60 s [*Pelgrum et al.*, 2011]. Also, a sliding averaging window was used, so that the rate of the indices is 1 Hz. It should be noted that although the GSV4004B receiver output S_4 and σ_ϕ measurements at 1/60 Hz rate, the values of the two indices used in this study were calculated from the high rate raw signal intensity and phase data in order to maintain consistency among different receivers (e.g., the PolaRxS does not output the values of S_4 and σ_ϕ indices). Calculation of the indices using high rate raw data also enables the customization of parameters, such as time interval, sliding window size, and low-pass delay correction. In addition, it should be mentioned that the conventional Butterworth detrending method may cause "phase without amplitude" scintillation phenomena frequently observed at high latitudes [*Forte and Radicella*, 2002; *Beach*, 2006; *Mushini et al.*, 2011]. In this study, the conventional detrending approach is taken to simply present the scintillation characteristics as observed by conventional receiver and processing methods.

In order to better characterize ionospheric scintillation, a set of criteria has been established to extract scintillation events from the data, based on evaluations of nonscintillation baseline indicators as described in the work of *Taylor et al.* [2012]. A brief summary and explanations of the criteria are listed as follows, and the reader is referred to *Jiao et al.* [2013c] and *Jiao* [2013] for more details.

1. The elevation angle mask is set to 30° to minimize multipath effects.
2. The thresholds for S_4 and σ_ϕ are 0.15 and 15° (0.26 rad), respectively, for data collected at Gakona. For equatorial data, the S_4 and σ_ϕ thresholds are 0.2 and 15°, respectively, to accommodate stronger amplitude scintillation.
3. To exclude certain interference cases, the index value needs to remain above the threshold value for a minimum of 30 s to qualify as a scintillation event.
4. An event detected within 5 min from the end of another event is not considered a new event. Instead, the two events are lumped into one event.
5. Scintillation events experienced by multiple satellites simultaneously are treated as separate events, and events experienced simultaneously by all tracked satellites are investigated on an individual basis to eliminate potential external interferences.
6. Carrier cycle slip ($\sigma_\phi > 100°$ (1.75 rad)) and loss-of-lock detection and repair procedures [*Liu*, 2011] are implemented. It can then be determined whether these cases are caused by scintillation or other factors (multipath or interference) using the previous criteria. These events are considered in the event duration statistics, but they are not included in the scintillation intensity statistics.

The criteria cited above are used to automate scintillation event extractions and are also designed to exclude most nonscintillation events (multipath and interference). The automated procedures greatly reduced the amount of time needed for visual inspection of individual events and enabled the generation of large number of scintillation events recorded at these three sites, which are necessary for statistical analysis and comparison of scintillation characteristics. It should be noted that these criteria and procedures involve some degrees of arbitration, and they are likely to introduce some errors in the classification of the observed events. To minimize the errors, they have been tested against a sample data set. Parameters used in the criteria were then selected based on extensive tests. Manual visual inspections are applied whenever there are cases of suspicious or difficult classification.

4. Results and Discussion

This section focuses on analyzing and comparing scintillation characteristics observed in high-latitude and equatorial regions using multifrequency GPS data collected during the 24th solar maximum. The high-latitude results presented here are based on a total of 5264 scintillation events determined using the criteria mentioned in section 3 from 1038 days' worth of L1C/A data collected in a time span of 4 years and 206 days' worth of L2C and L5 data during a span of 8 months. For equatorial scintillation, 7690 events from Jicamarca, Peru, and 129 scintillation events from Ascension Island were observed and analyzed for a total of 332 days' worth of data from 2012 to 2014. The detailed number of amplitude and phase scintillation events observed at the three locations are listed in Table 4.

4.1. Scintillation Indicator and Duration Distributions

The magnitudes of the two scintillation indices, S_4 and σ_ϕ, are often used to indicate the intensity of ionospheric scintillation, as their values directly reflect the disturbance magnitudes of received power and carrier phase measurements. Figure 3 compares GPS L1C/A, L2C, and L5 intensity distributions of amplitude and phase scintillation observed at Gakona, Jicamarca, and Ascension Island. MaxS_4 or maxσ_ϕ in the figures is the maximum S_4 or σ_ϕ value during an amplitude or phase scintillation event, which is a practical indicator of the impact of scintillation on GNSS receivers. Note that due to the limited number of events observed on L2C and L5 from Ascension Island, statistical results are not presented for them in Figures 3c–3f.

Figure 3a shows that amplitude scintillation events observed on L1C/A in the equatorial region were generally more intense than those observed at Gakona. This is consistent with most previous studies, which concluded that amplitude scintillation is most intense in the equatorial region [*Basu et al.*, 2002]. Figure 3b shows that the magnitudes of L1C/A phase fluctuations at Jicamarca and Gakona are comparable. On Ascension Island, more deep amplitude and large phase variations including cycle slips were observed in the data, resulting in higher probabilities of larger maxS_4 and maxσ_ϕ. Also, note that there is a limited amount of data from Ascension Island, which impacts the statistical soundness of the probability distributions. The sampling pools for scintillation on L2C and L5 are even more limited compared to those for L1C/A. This is especially true for amplitude scintillation at high latitudes, resulting in the rough appearance of the distributions in Figures 3c, 3e, and 3f.

To further illustrate the relationship of the index values across the three GPS bands, Figure 4 gives three examples observed on PRN 1 on 17 March 2013 at Gakona, on PRN 25 on 5 October 2013 at Jicamarca, and on PRN 24 on 10 March 2013 on Ascension Island. The red solid lines in the plot are least-mean-square linear fits that intercept the origin. The slopes of the linear fits are marked in each subplot as r values. The linear fit is based on the theory that the scintillation index values follow a power law dependence on frequency, assuming that the scintillation is caused by a weak scattering through a thin, phase-changing screen [*Rino*, 1979a, 1979b; *Franke et al.*, 1984; *Van Dierendonck et al.*, 1993]. To reduce the impact of multipath, receiver noise, and scintillation saturation effect on the linear fit, only signals above 20° elevation with S_4 values between 0.1 and 0.8 or σ_ϕ values between 10° and 40° are included. Figure 4 shows that L2C and L5 signals are more adversely affected during scintillation than L1C/A signal. However, the quantitative relationship of the scintillation indices on signal frequency varies for different times, receiver location, and the satellite. Figure 4a shows that although there are strong phase scintillation at Gakona on PRN 1, there was hardly any amplitude scintillation observed. In Figure 4c, the data points are more spread at higher scintillation indices, indicating the breakdown of the power law dependence and the effects of scintillation saturation during strong scintillation.

Apart from the magnitude, the duration of a scintillation event can also indicate its severity and its negative impact on receiver signal processing and the navigation solution's accuracy, integrity, and availability. Therefore, event duration probability distributions of amplitude and phase scintillation are shown in Figure 5, with the mean values indicated in the legends. The duration of an event is defined as the difference between the ending time and the starting time of the event that satisfies the criteria listed in section 3. No statistical analysis is presented for Ascension Island in Figures 5c–5f due to a lack of a sufficient number of events to be statistically significant. Figure 5 shows that equatorial scintillation events generally lasted longer than those at high latitudes. At Gakona, observed phase scintillation generally lasted longer than amplitude scintillation,

Table 4. Amplitude and Phase Scintillation Event Number Observed Using Criteria Described in Section 3 and Analyzed in Section 4 on Three GPS Bands at Gakona, Alaska, Jicamarca, Peru, and Ascension Island

Event No.

Band	L1C/A		L2C		L5		
Location	Amplitude	Phase	Amplitude	Phase	Amplitude	Phase	Total
Gakona, Alaska	1271	3617	63	243	18	52	5264
Jicamarca, Peru	2438	2795	885	830	366	376	7690
Ascension Island	31	66	11	13	3	5	129

except on L5, mainly due to a lack of observations because only a few GPS satellites were broadcasting L5 signals. At Jicamarca, however, amplitude scintillation events lasted longer than the phase scintillation events. On average, Ascension Island observed the longest scintillation events on L1C/A among the three sites, although more data are needed to further confirm this result. In addition, at both Gakona and Jicamarca, events

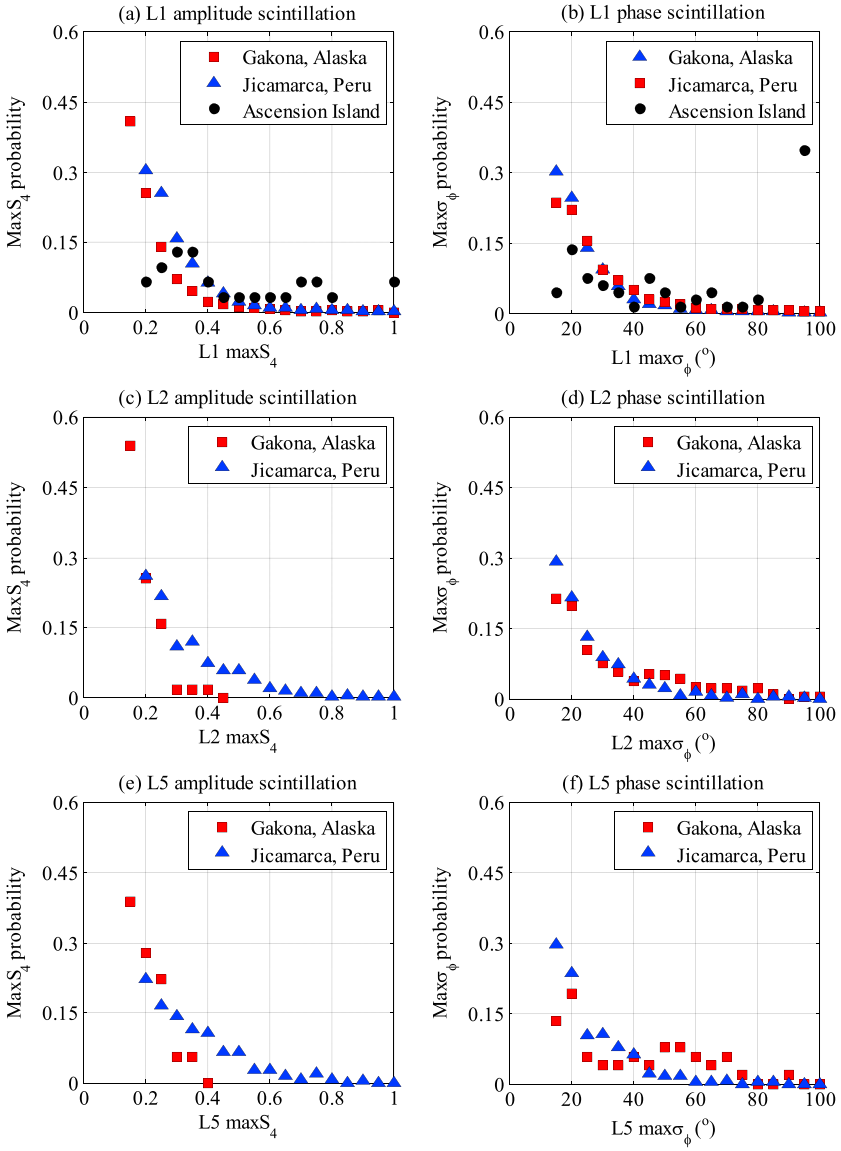

Figure 3. Distributions of maxS_4 and maxσ_ϕ (maximum S_4 and σ_ϕ during an event) for amplitude and phase scintillation on L1C/A, L2C, and L5 observed at Gakona (Alaska), Jicamarca (Peru), and Ascension Island. Statistical analysis is not presented for L2C and L5 data from Ascension Island due to a limited number of events.

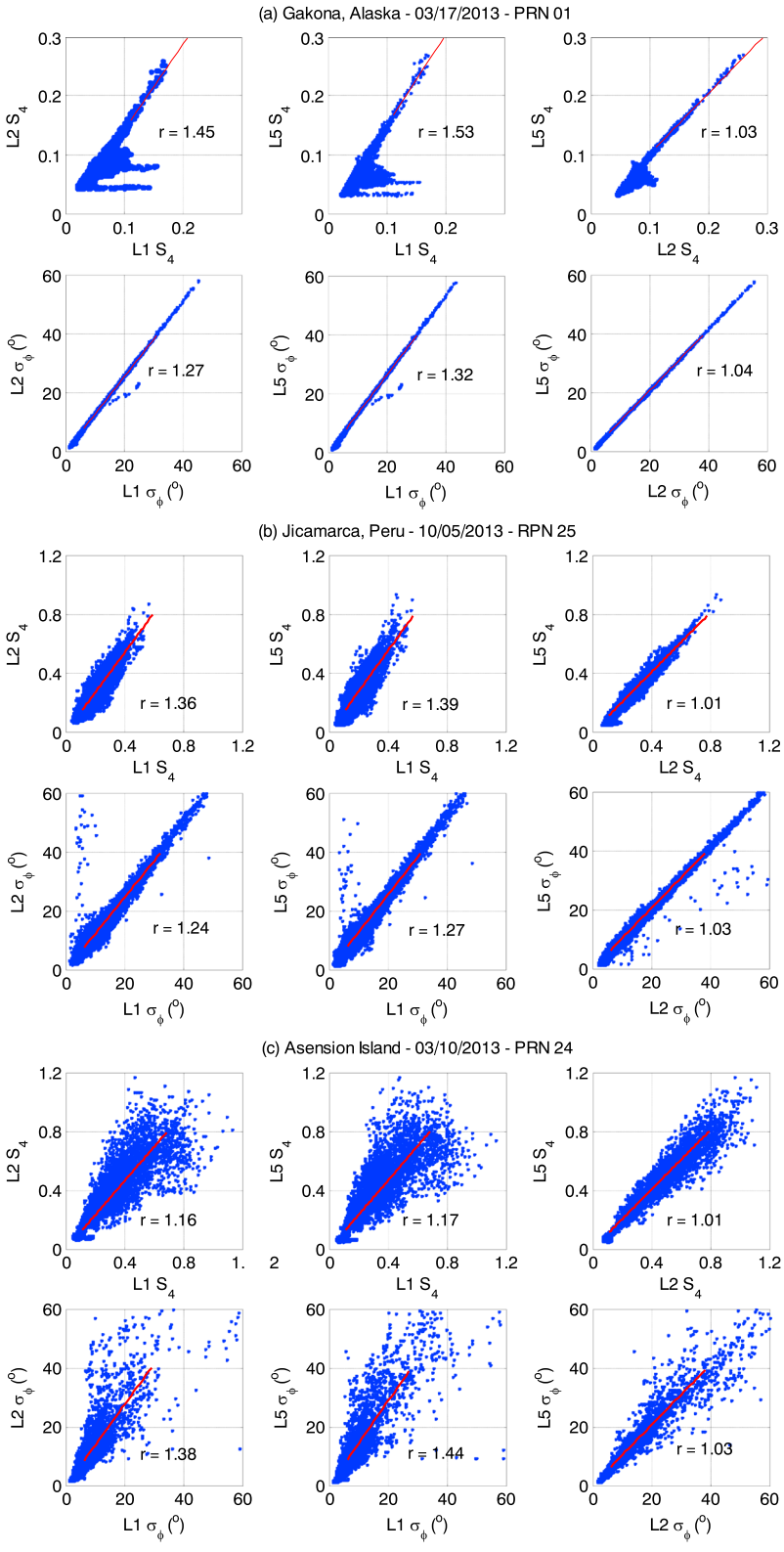

Figure 4. Examples of the relationship of S_4 and σ_ϕ indices across the GPS bands at (a) Gakona, Alaska on PRN 1 on 17 March 2013; (b) Jicamarca, Peru, on PRN 25 on 5 October 2013; and (c) Ascension Island on PRN 24 on 10 March 2013. The indices are calculated within 10 s intervals for signals above 20° elevation. The *r* values denoted in the plot are the slope rates of the linear-fit lines which intercept the origin. For S_4 index, the linear fit is conducted using points between 0.1 and 0.8. For σ_ϕ index, the linear fit is conducted using points between 10° and 40°.

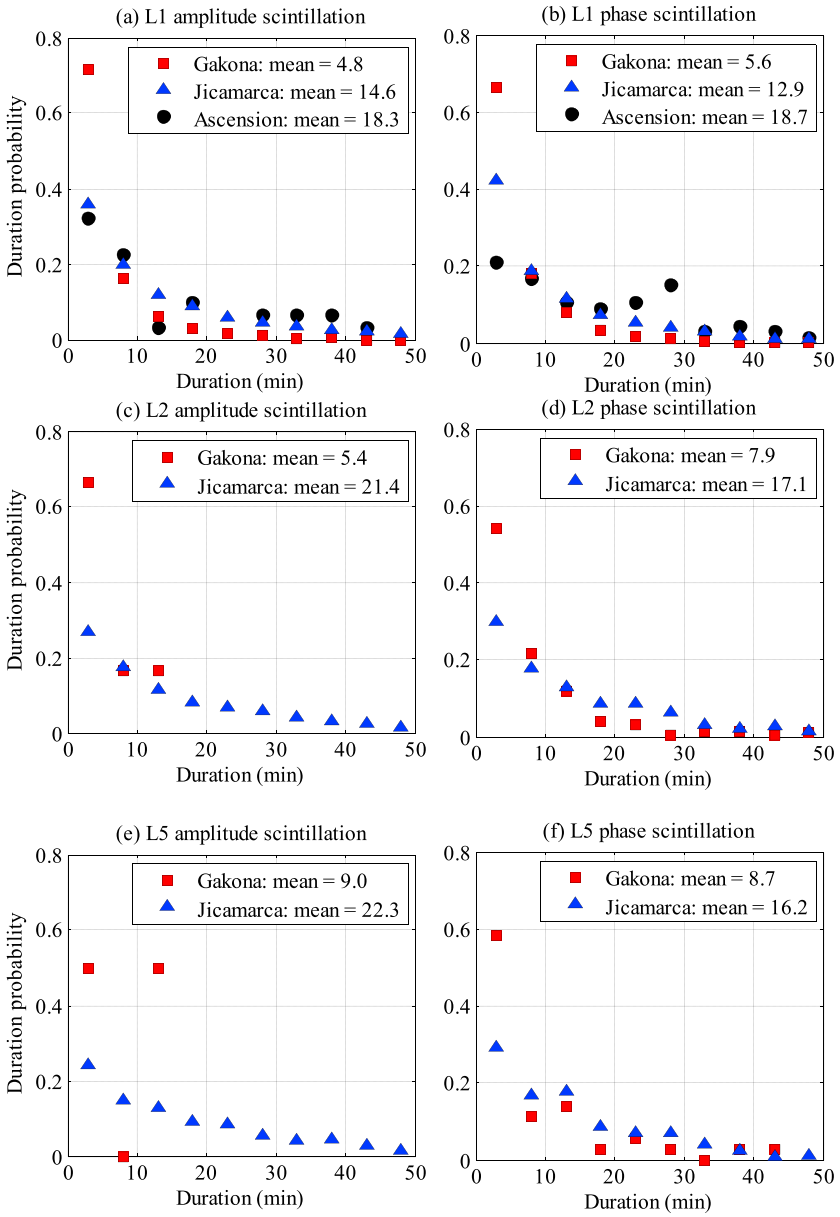

Figure 5. Duration distributions of amplitude and phase scintillation events on L1C/A, L2C, and L5 observed at Gakona (Alaska), Jicamarca (Peru), and Ascension Island. Statistical analysis is not presented for L2C and L5 data from Ascension Island. Mean duration values are labeled in the legends.

on L5 are generally longer than those on L2C, which in turn are longer than those on L1C/A, with the exception of phase scintillation at Jicamarca where the mean L2C duration is actually slightly longer than that of L5.

Ionospheric scintillation of combined high intensity and long duration poses a major threat to signal processing in GNSS receivers [*Seo et al.*, 2009, 2011]. Unfortunately, these two aspects are often positively correlated at equatorial locations and high latitudes especially during active solar and geomagnetic activities. Moderate correlation coefficients (0.5–0.7) [*Rumsey*, 2011] have been observed between scintillation durations and the magnitudes of scintillation indicators at both Jicamarca and Ascension Island (Figures 6b and 6c). The correlations, however, are much smaller at Gakona, especially for amplitude scintillation events. Because simultaneous deep amplitude fading and large phase variations impose conflicting demands on receiver carrier tracking loop design, these results further confirm that scintillation is a more challenging issue for receiver design in the equatorial region.

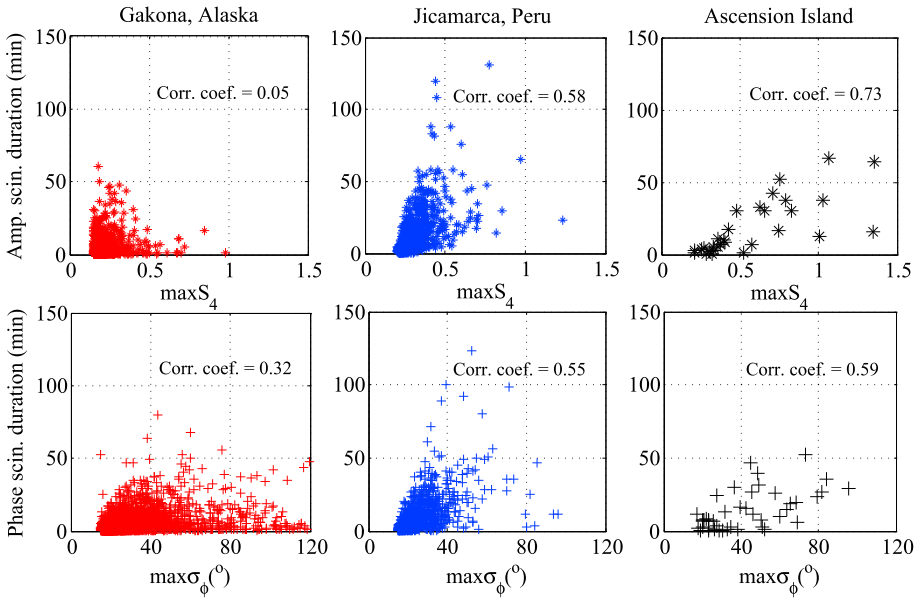

Figure 6. Scintillation duration versus intensity and their correlation coefficients on L1C/A for (top row) amplitude and (bottom row) phase scintillation events at (left column) Gakona, (middle column) Jicamarca, and (right column) Ascension Island.

4.2. Diurnal and Seasonal Dependency of Scintillation Occurrence

The occurrence frequency of scintillation events, defined as the number of scintillation events recorded based on the criteria described in section 3 during a certain time interval, is an important indicator in scintillation climatology studies [*Alfonsi et al.*, 2011; *Prikryl et al.*, 2011]. The knowledge of the occurrence frequency dependence on time and season can help to predict the periods when scintillation is most likely to occur.

Figure 7 shows scintillation hourly occurrence probabilities at the three sites with respect to hours after local sunset. Although scintillation events at the three locations mostly occurred during local nighttime, the distribution at high latitudes is much flatter than those in the equatorial region, where the events are mostly concentrated between 1–2 h post local sunset and midnight. Statistics show that more than 98% of the scintillation at Jicamarca and Ascension Island was observed from 1 to 6 h after sunset, which is consistent with previous findings [*Basu et al.*, 2002; *Cervera and Thomas*, 2006; *Beniguel et al.*, 2009].

In addition to solar radiation, scintillation occurrence is also affected by the Earth's orientation and the Sun-Earth magnetic field interaction, which is reflected in the seasonal pattern of scintillation. Figure 8 illustrates how scintillation occurrence frequency at Gakona and Jicamarca was affected by solar activity and seasons. The four seasons are defined as spring, March to May; summer, June to August; fall, September to November; and winter, December to February. The mean event number for a season is the total number of events observed in that season divided by the percentage of data available during the period (shown as the percentages in Tables 1 and 2). The intensity of solar activity is indicated by the seasonal sum of the monthly sunspot number shown as the black dotted line.

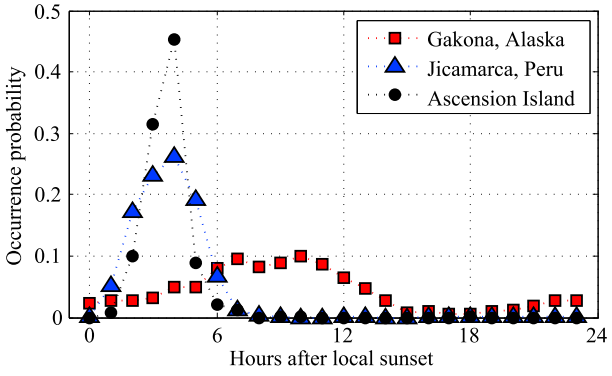

Figure 7. Scintillation occurrence frequency on L1C/A with respect to hours after local sunset at Gakona, Jicamarca, and Ascension Island.

Due to the limited data sets available from these two sites, it is difficult to make a clear comparison until more data are

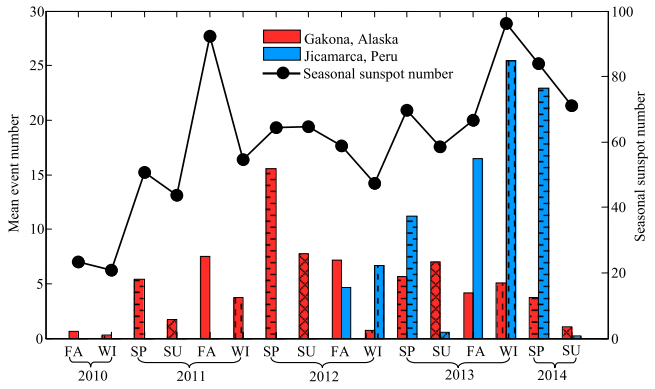

Figure 8. Seasonal scintillation occurrence frequency on GPS L1C/A, determined by the mean event number (the histogram), compared with the seasonal sunspot number (the black dotted line) for Gakona and Jicamarca.

processed. Nevertheless, several observations can be made from the individual data sets. At Gakona, the scintillation occurrence frequency is correlated primarily with sunspot numbers. There is also a secondary seasonal modulation effect. Scintillation was observed more frequently in spring and fall than in summer and winter. In contrast to the half-a-year cycle at high latitudes, at Jicamarca, scintillation follows a 1 year cycle, as described in previous research [*Akala et al.*, 2011], and is largely subdued in the summer.

4.3. Scintillation and Geomagnetic Activity

Ionospheric scintillation is closely related to interplanetary magnetic field and geomagnetic field disturbances, especially in high-latitude regions [*Basu et al.*, 2002; *Rodrigues et al.*, 2004; *Prikryl et al.*, 2010, 2011; *Jiao et al.*, 2013b]. Therefore, data collected during solar or geomagnetic storms are of great interest, as strong scintillation events are more likely to be observed at high latitudes. Since 2011, we have entered the 24th solar maximum during which solar activities are expected to be at their peak level at the time of this writing. However, because of a dip in solar activity in 2012, only a few days in 2011, 2012, and 2013 experienced large geomagnetic disturbances. Table 5 lists the days from 2011 to 2013 when *Ap* index values reached or exceeded 27 (corresponding to $Kp \geq 4$). On seven of the days, the average geomagnetic activity reached storm level according to the NOAA space weather scale ($Kp \geq 5$). Note that some GPS data from Alaska and Peru are missing due to system outages; also, HAARP magnetometer readings on some days are not available. Finally, data collected on Ascension Island are only discussed in section 4.3.2 due to the limited time span of the data.

Table 5. Days From 2011 to 2013 With $Ap \geq 27$ ($Kp \geq 4$)

Date		*Ap*	*Kp*	Date		*Ap*	*Kp*
2011	03/01	27	4	2012	07/15	78	6−
	03/11	37	4+		07/16	42	5−
	05/28	45	5−		09/03	31	4
	05/29	34	4+		09/05	32	4+
	08/05[a]	42	5−		10/01	32	4+
	08/06[a]	31	4		10/08	40	5−
	09/09[a]	30	4		10/09	46	5−−
	09/10[a]	40	5−		10/13	47	5−
	09/12[a]	27	4		11/14	37	4+
	09/17[a]	32	4+	2013	03/01[b]	34	4+
	09/26[a]	38	4+		03/17[b]	72	6−
	09/27[a]	30	4		03/29[b]	28	4
	10/25[a]	38	4+		05/01[a,b]	29	4
2012	03/07[a]	48	5		05/25	37	4+
	03/09	87	6		06/01	58	5+
	03/12	32	4+		06/07[b,c]	27	4
	03/15	36	4+		06/29[c]	50	5
	04/24[a]	41	5−		07/06[c]	27	4
	04/25[a]	27	4		10/02[c]	58	5+
	06/17	43	5−		10/09[c]	29	4
	07/09	42	5−		12/08[c]	28	4

[a]Days without Alaska GPS data;
[b]Days with Peru GPS data;
[c]Days without HAARP geo-magnetometer data.

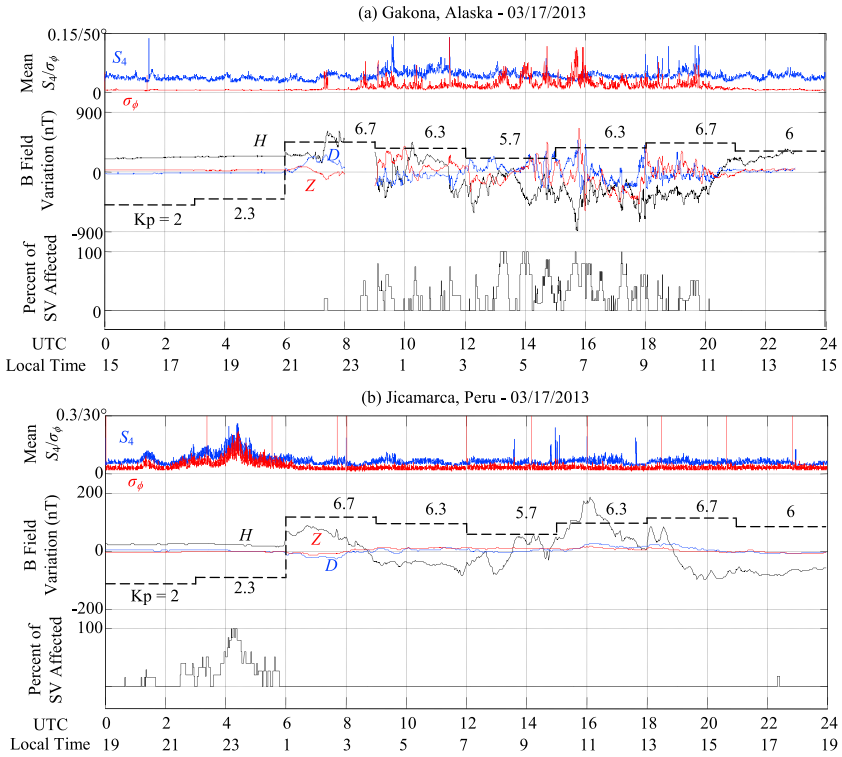

Figure 9. Scintillation on L1C/A and geomagnetic field activities observed at (a) Gakona, Alaska, and (b) Jicamarca, Peru, on 17 March 2013 [*Jiao et al.*, 2013b]. The two curves on the top of each subplot are S_4 (blue) and σ_ϕ (red) values averaged among all the satellites above 30° with upper bounds limited to show details. The three curves below S_4 and σ_ϕ in each subplot are readings from the magnetometer of the *H*, *D*, and *Z* components of the local geomagnetic field. The dashed stair line imposed on them is the *Kp* index for global geomagnetic activity. The stair line on the bottom in each subplot shows the percentage of satellites (SV) affected by scintillation above the elevation of 30°.

4.3.1. A Case Study Example

In order to illustrate and compare the qualitative relationship between ionospheric scintillation and geomagnetic disturbances observed in high-latitude and equatorial regions, a case study was conducted based on data collected on 17 March 2013 (Figure 9) [*Jiao et al.*, 2013b]. At the top of both subplots Figures 9a and 9b are average S_4 and σ_ϕ indices on L1C/A among satellites above 30° elevation. Spikes in the curves are caused by loss-of-lock of at least one satellite signal. The stair line on the bottom of each subplot represents the percentage of satellites affected at a given epoch with elevation above 30°. Finally, each subplot also accommodates zero-mean variations of the *H*, *D*, and *Z* components of the local geomagnetic field. Outages of the HAARP magnetometer led to discontinuities in the curves in Figure 9a at around 23:00 and 14:00 local time. In order to show the intensity of the global geomagnetic field activity, 3 h *Kp* values are plotted over the *H*, *D*, and *Z* curves. Both UTC and local time are shown on the horizontal axis.

Figure 9 shows that at both locations the local geomagnetic field disturbances started at approximately 6 h UTC. At Gakona, the intensity of ionospheric scintillation, especially phase scintillation, increased as the local geomagnetic field disturbance became enhanced. It can also be observed at Gakona that the percentage of satellites affected was highly synchronized with disturbances in geomagnetic field components, which indicates that scintillation and local geomagnetic field activities are strongly correlated in Alaska [*Aquino et al.*, 2005]. In contrast, scintillation at Jicamarca is much less correlated with geomagnetic activity with most events observed before the storm from 2.5 to 6 h UTC. In all, it can be concluded from Figure 9 that disturbances in the geomagnetic field do not correlate with scintillation in the equatorial region as they do at high latitudes. This conclusion is in agreement with conclusions from earlier studies that solar and geomagnetic activities only play a secondary modulating role in equatorial scintillation [*Basu et al.*, 2002].

4.3.2. Ionospheric Scintillation and Global Geomagnetic Field Activities

To obtain a more general relationship between ionospheric scintillation and global geomagnetic field activity, possible correlation between daily scintillation occurrence frequency and daily geomagnetic activity

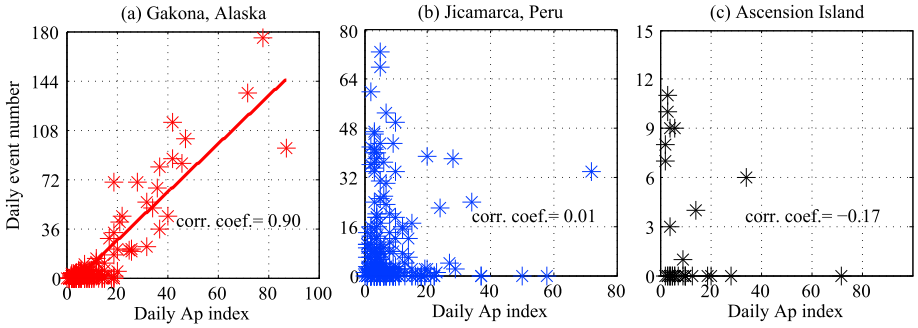

Figure 10. Daily scintillation event occurrence frequency on L1C/A with respect to *Ap* index at (a) Gakona, Alaska; (b) Jicamarca, Peru; and (c) Ascension Island. A linear least-mean-square fit is imposed on subplot Figure 10a based on the data points.

index *Ap* is presented in Figure 10. The result in Figure 10a was obtained using data collected over seven months at Gakona: March and November 2011, March, July, October and November 2012, and March 2013. During these months, scintillation and geomagnetic field activities were relatively high. For equatorial results shown in Figures 10b and 10c, all the data from November 2012 to June 2013 (8 months) were analyzed for Jicamarca, and all 10 days' data from 1 to 10 March in 2013 were analyzed for Ascension Island.

Figure 10 shows a strong correlation between occurrence frequency of scintillation events and *Ap* index values at Gakona with a correlation coefficient of 0.90. In contrast, the correlation coefficients are negligible in the equatorial region, indicating that equatorial scintillation is relatively independent of global geomagnetic activity.

4.3.3. High-Latitude Ionospheric Scintillation and Local Geomagnetic Field Activities

Although the *Kp* and *Ap* indices discussed in the previous section are closely related to the scintillation observed at Gakona, they do not necessarily reflect activities in the local geomagnetic field as these indices are 3 hour averages among observations from 13 geomagnetic observatories located around the world [*Bartels et al.*, 1939; *Rostoker*, 1972; *Mayaud*, 1980]. Therefore, readings from the co-located geomagnetometer are used to further investigate any correlation between ionospheric scintillation and local geomagnetic field activities. Note that all results discussed in this section are only for L1C/A data collected at Gakona, as the amount of correlation has been insignificant in the equatorial region as shown in Figures 9 and 10.

Figure 11 investigates the correlation between the hour-by-hour magnitude of the local geomagnetic field standard deviation and the S_4/σ_ϕ index, averaged among all satellites above the elevation of 30° (excluding the satellite signals that lost lock). The investigation is based on data collected on the 23 days listed in Table 5

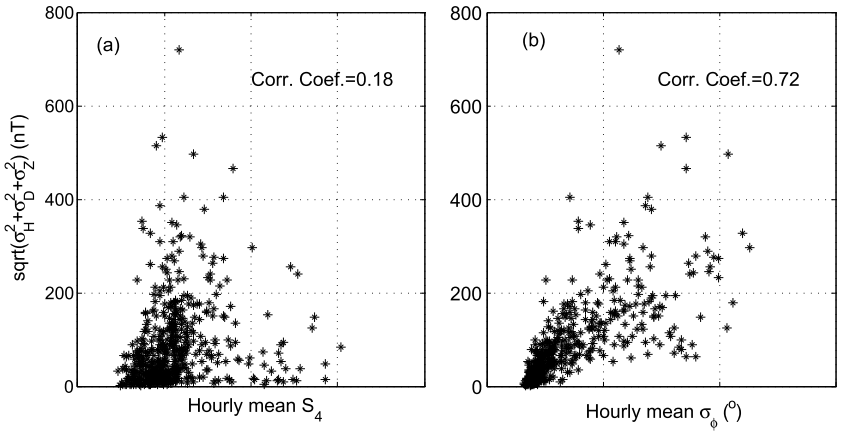

Figure 11. Correlation between hour-by-hour magnitude of the local geomagnetic field standard deviation and average L1C/A S_4/σ_φ index over all SV above 30° elevation at Gakona, Alaska. Correlation coefficients are labeled in both subplots.

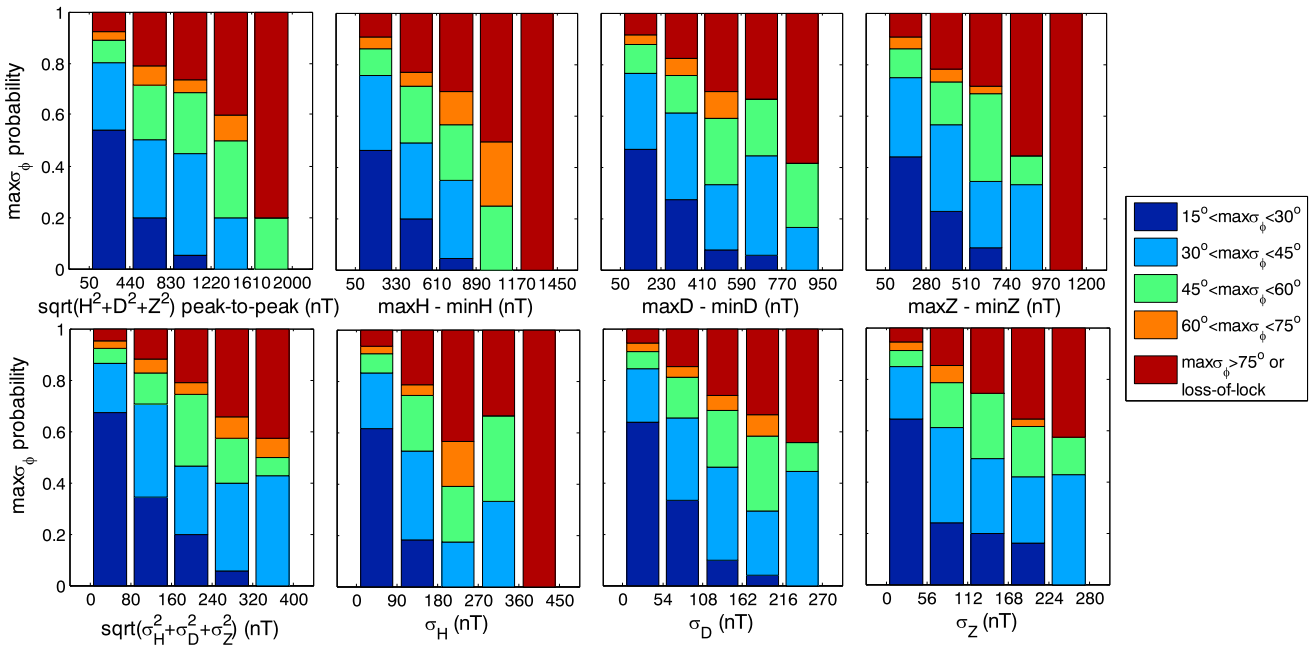

Figure 12. Event-based L1C/A maxσ_ϕ occurrence probability on variations in geomagnetic field amplitudes and standard deviations in geomagnetic field components in Alaska. The statistics are conducted by categorizing the maximum value of the σ_ϕ index during an event (the color bar) with respect to (top row) the peak-to-peak geomagnetic field component readings or (bottom row) the deviations in field component readings during the event. The top row shows that the larger the change in the magnitude of geomagnetic field, the more likely it is to observe stronger phase scintillation. The bottom row shows that the more rapid the change in the local geomagnetic field, the more likely it is to observe stronger phase scintillation.

with a daily equivalent $Kp \geq 4$ when both GPS and geomagnetometer data were available. The magnitude of the geomagnetic field standard deviation is nearly linearly related to the hourly mean σ_ϕ as shown in subplot Figure 11b with the correlation coefficient of 0.72, whereas its relationship with the hourly mean S_4 index is fairly weak with a correlation coefficient of 0.18. Additional data analysis also shows a similar correlation between standard deviations in individual field components and average S_4/σ_ϕ index values. These results show that at Gakona, geomagnetic field disturbances are much more strongly correlated with phase scintillation than with amplitude scintillation. Furthermore, the relatively moderate correlation coefficient values for phase scintillation indicate that there must be other factors influencing scintillation occurrence and severity at high latitudes.

A more striking way to demonstrate the relationship between geomagnetic field disturbance and the level of phase scintillation is shown in Figure 12. The statistics are conducted by categorizing the maximum value of the σ_ϕ index during an event (the color bar) with respect to the peak-to-peak geomagnetic field component readings (Figure 12, top row) and the deviations in field component readings (Figure 12, bottom row) during the event. In addition to the days listed in Table 5, events on 10 March and 1 November in 2011, 15 February and 1 November 2012 are also included in this plot. From these 27 days of data, there are 1505 phase scintillation events, 25 amplitude scintillation events, and 158 concurrent amplitude and phase scintillation events. Considering the weak correlation observed in Figure 11 and the smaller number of events, amplitude scintillation is not discussed in Figure 12.

The top row of Figure 12 shows that the larger the change in the magnitude of geomagnetic field, the more likely it is to observe stronger phase scintillation. The bottom row shows that the more rapid the change in the local geomagnetic field, the more likely it is to observe stronger phase scintillation. It can also be seen in Figure 12 that the same phenomenon can be observed not only in the magnitude of the geomagnetic field, but also in individual field components. In addition, Figure 13 presents quantitative relationships between the occurrence probability of phase scintillation events with maxσ_ϕ values larger than 30°, and the variation and deviation in the geomagnetic field. The statistics in Figure 13 are obtained by summing the probabilities of max$\sigma_\phi > 30°$ in Figure 12, so that each bar in Figure 12 becomes a data point in Figure 13, and the two subplots correspond to the top row and the bottom row in Figure 12, respectively. Based on the

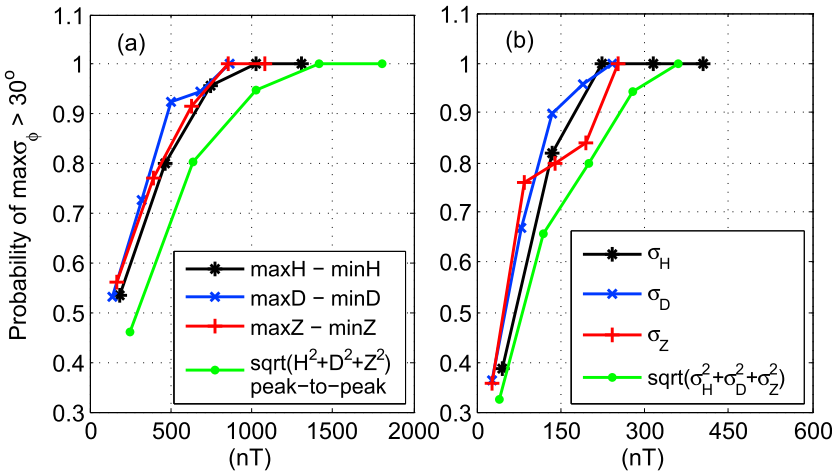

Figure 13. Event-based occurrence probability of max$\sigma_\varphi > 30°$ on L1C/A with respect to (a) variations in geomagnetic field amplitudes and (b) standard deviations in geomagnetic field components in Alaska. The statistics are obtained by summing the probabilities of max$\sigma_\varphi > 30°$ in Figure 12, so that each bar in Figure 12 becomes a data point in this figure. The two subplots correspond to the top row and the bottom row in Figure 12, respectively.

occurrence probability shown in Figure 13, the disturbances in the local geomagnetic field can be used in future research to predict the intensity of phase fluctuations observed in Alaska.

5. Summary and Recommendations for Future Work

This paper compares different features of ionospheric scintillation in high-latitude and equatorial regions, using high-rate, multifrequency GPS data collected during the 24th solar maximum at Gakona, Alaska, Jicamarca, Peru, and Ascension Island. More than 5000 high-latitude and 8000 equatorial scintillation events have been used to investigate various aspects of scintillation characteristics across the GPS signal bands at the three antenna sites. Scintillation intensity, duration, occurrence frequency, seasonal pattern, and its relationship to solar and geomagnetic activities were the main variables investigated. The results of this work provide a supportive and comprehensive analysis of when and how scintillation occurs in the northern auroral and equatorial regions and can help with future scientific research on GNSS receiver design for robust signal tracking and monitoring of space weather. A summary of the results also substantiate the following conclusions in general scintillation studies by means of quantitative analysis:

1. Scintillation in the equatorial region is typically more severe than that at high latitudes with deeper and faster signal power fading and longer duration. Equatorial scintillation with higher intensity usually lasts longer, which further contributes to its pronounced impact on signal acquisition and tracking in receivers. In addition, scintillation is generally more intense and longer lasting on Ascension Island than at Jicamarca, Peru.
2. In the high-latitude region, phase fluctuations are more severe than amplitude scintillation. There are a larger number of phase fluctuations having longer durations compared to the relatively mild-amplitude scintillation. We emphasize that the different amplitude and phase scintillation thresholds used in this study do not affect this conclusion. The lower amplitude scintillation threshold used to extract high-latitude scintillation is intended to preserve as many amplitude scintillation events as possible.
3. Scintillation events are generally stronger and longer-lasting on L2C and L5 than on L1C/A at both high-latitude and equatorial regions. A more detailed analysis of multifrequency equatorial scintillation is the subject of another publication by the same authors.
4. Scintillation occurs more frequently during nighttime, and almost all equatorial scintillation events were observed to occur within 6 h after local sunset. The overall occurrence frequency of scintillation not only increases with an increase in solar activity but also follows certain seasonal patterns at different geographic locations. In general, scintillation effects are more pronounced during equinoxes.
5. Occurrence frequency of scintillation observed in Alaska has a strong positive relationship with global geomagnetic field activity. More scintillation events are likely to be observed when the *Ap*/*Kp* index is larger. On the other hand, equatorial scintillation activity is largely independent of geomagnetic activity.

6. In Alaska, the magnitude and rate of fluctuations in the local geomagnetic field are strongly correlated with the intensity of phase scintillation events. Larger and more rapidly changing disturbances in the geomagnetic field are generally associated with phase scintillation events of stronger intensity. However, such correlation is much weaker for amplitude scintillation. It should also be noted here that the 24th solar cycle is a relatively mild one. Because of this the relationship between geomagnetic activity and scintillation effects derived from the data in this study may prevent it from being extended in a generalized way to all situations.

The above conclusions are drawn from a preliminary study. But they offer promise for the future development of high-latitude and equatorial ionospheric scintillation forecasting and prediction. As more data become available from an increasing number of monitoring sites, especially from equatorial regions, a more comprehensive analysis and comparison can be made to facilitate global scintillation monitoring, mapping, and modeling.

The establishment of criteria to identify and quantify scintillation events is essential for automated processing of massive amount of data collected from multiple stations during the 24th solar maximum. The criteria are defined to minimize false alarms due to interferences, multipath, and other nonscintillation-related disturbances on GPS signals. There are necessary arbitrary elements in the event selection criteria. Additionally, carrier phase cycle slips during strong scintillation introduce errors in phase scintillation characterization. Although every effort was made to detect and repair cycle slips in the data presented in this study, there are outstanding challenges in separating actual phase jumps associated with deep amplitude fading from artificial cycle slips introduced by receiver processing [*Humphreys et al.*, 2010; *Xu and Morton*, 2015]. The ultimate solution is to eliminate or drastically reduce the number of cycle slips through development of robust carrier tracking algorithms and application of these algorithms to postprocess raw IF data collected during strong scintillation events. To facilitate this approach, scintillation event-driven raw IF scintillation data collection systems have been developed and deployed at several equatorial and high-latitude locations [*Morton et al.*, 2015].

Recent progress in receiver algorithm development specifically designed to capture carrier parameter distortions during scintillation shows promise in generating accurate and reliable scintillation indicators, which will improve future studies of scintillation characteristics [*Xu and Morton*, 2015; *Yin et al.*, 2014]. As satellite navigation becomes increasingly important in many civil and defense applications, ionospheric scintillation will impact the accuracy, availability, and integrity of GPS receiver performance. Scintillation signal characteristics revealed by the studies presented in this paper and elsewhere offer important guidelines in next-generation GPS receiver algorithm development that can mitigate scintillation effects to provide robust navigation solutions and to function as effective distributed sensors for ionosphere and space weather monitoring.

Acknowledgments

The GPS data for this paper were collected by the authors research team, and the data collection systems at Gakona and Ascension Island are sponsored by the Air Force Research Laboratory, Reference Systems Branch at Wright Patterson Air Force Base, while the Jicamarca system was established with funding support from Consortium of Ohio Universities on Navigation and Timekeeping (COUNT). The Gakona geomagnetic data were provided by Michael McCarrick of the Naval Research Laboratory and by Alaska Satellite Facility. The latter can be downloaded from https://www.asf.alaska.edu/magnetometer/download/#gakona. The Jicamarca geomagnetic data were provided by Ramiro Yanque of Jicamarca Radio Observatory. The archived global geomagnetic *Kp* and *Ap* index values are available on NOAA website at ftp://ftp.ngdc.noaa.gov/STP/GEOMAGNETIC_DATA/INDICES/KP_AP. This research was supported by a start-up fund from Colorado State University and AFOSR grant #FA9550-14-1-0265. The authors appreciate the support of the HAARP staff and the Geophysical Institute at the University of Alaska Fairbanks for on-site support of the GNSS receiver data collection system. The Jicamarca Radio Observatory is a facility of the Instituto Geofisico del Peru operated with support from the NSF AGS-0905448 through Cornell University. The authors would also like to acknowledge Jicamarca Radio Observatory for hosting the GNSS receiver and providing the magnetometer data. Todd Pedersen from Air Force Research Laboratory at Kirkland AFB and Miami University graduate students Steve Taylor and Harrison Bourne made it possible to collect the GPS scintillation data on Ascension Island.

References

Aarons, J. (1982), Global morphology of ionospheric scintillation, *Proc. IEEE*, *70*, 360–378, doi:10.1109/PROC.1982.12314.

Aarons, J., and S. Basu (1994), Ionospheric amplitude and phase fluctuations at the GPS frequencies, Proceedings of the 7th International Technical Meeting of the Satellite Division of The Institute of Navigation (ION GPS 1994), 1569–1578, Salt Lake City, Utah.

Akala, A. O., P. H. Doherty, C. E. Valladares, C. S. Carrano, and R. Sheehan (2011), Statistics of GPS scintillations over South America at three levels of solar activity, *Radio Sci.*, *46*, RS5018, doi:10.1029/2011RS004678.

Alfonsi, L., L. Spogli, G. De Franceschi, V. Romano, M. Aquino, A. Dodson, and C. N. Mitchell (2011), Bipolar climatology of GPS ionospheric scintillation at solar minimum, *Radio Sci.*, *46*, RS0D05, doi:10.1029/2010RS004571.

Aquino, M., T. Moore, A. Dodson, S. Waugh, J. Souter, and F. S. Rodrigues (2005), Implications of ionospheric scintillation for GNSS users in norhtern Europe, *J. Navigation*, *58*(2), 241–256, doi:10.1017/S0373463305003218.

Azeem, I., G. Crowley, A. Reynolds, J. Santana, and D. Hampton (2013), First results of phase scintillation from a longitudinal chain of ASTRA's SM-211 GPS TEC and scintillation receivers in Alaska, Proc. ION PNT, 735–742, Honolulu, Hawaii.

Bartels, J., N. H. Heck, and H. F. Johnston (1939), The three-hour range index measuring geomagnetic activity, *J. Geophys. Res.*, *44*, 411–454, doi:10.1029/TE044i004p00411.

Basu, S., K. Grovesa, S. Basu, and P. Sultana (2002), Specification and forecasting of scintillations in communication and navigation links: Current status and future plans, *J. Atmos. Sol. Terr. Phys.*, *64*, 1745–1754, doi:10.1016/S1364-6826(02)00124-4.

Beach, T. L. (2006), Perils of the GPS phase scintillation index (Sigma Phi), *Radio Sci.*, *41*, RS5S31, doi:10.1029/2005RS003356.

Beniguel, Y., V. Romano, L. Alfonsi, M. Aquino, et al. (2009), Ionospheric scintillation monitoring and modelling, *Ann. Geophys.*, *52*, 391–416, doi:10.4401/ag-4595.

Briggs, B. H., and I. A. Parkin (1963), On the variation of radio star and satellite scintillations with zenith angle, *J. Atmos. Terr. Phys.*, *25*, 339–366, doi:10.1016/0021-9169(63)90150-8.

Buchau, J., E. J. Weber, D. N. Anderson, H. C. Carlson Jr., J. G. Moore, B. W. Reinisch, and R. C. Livingston (1984), Ionospheric structures in the polar cap: Their origin and relation to 25-MHz scintillation, *Radio Sci.*, *20*(3), 325–338, doi:10.1029/RS020i003p00325.

Carroll, M., Y. Morton, and E. Vinande (2014), Triple frequency GPS signal tracking during strong ionospheric scintillations over Ascension Island, *Position, Location and Navigation Symposium - PLANS 2014, 2014 IEEE/ION*, 43–49, doi:10.1109/PLANS.2014.6851356.
Cervera, M. A., and R. M. Thomas (2006), Latitude and temporal variation of equatorial ionospheric irregularities determined from GPS scintillation observations, *Ann. Geophys.*, *24*, 3329–3341, doi:10.5194/angeo-24-3329-2006.
Dagg, M. (1957), The correlation of radio-star-scintillation phenomena with geomagnetic disturbances and the mechanism of motion of the ionospheric irregularities in the F region, *J. Atmos. Terr. Phys.*, *10*, 194–203, doi:10.1016/0021-9169(57)90086-7.
Das Gupta, A., A. Maitra, and S. K. Das (1985), Post-midnight scintillation activity in relation to geomagnetic disturbances, *J. Atmos. Terr. Phys.*, *47*, 911–916, doi:10.1016/0021-9169(85)90067-4.
De Franceschi, G., L. Alfonsi, and V. Romano (2006), Isacco: An Italian project to monitor the high latitude ionosphere by means of GPS receivers, *GPS Solut.*, *10*, 263–267, doi:10.1007/s10291-006-0036-6.
Forte, B., and S. M. Radicella (2002), Problems in data treatment for ionospheric scintillation measurements, *Radio Sci.*, *37*(6, 1096), doi:10.1029/2001RS002508.
Fortes, L. P. S., T. Lin, and G. Lachapelle (2014), Effects of the 2012–2013 solar maximum on GNSS signals in Brazil, *GPS Solut.*, *19*(2), 309–319, doi:10.1007/s10291-014-0389-1.
Franke, S. J., C. H. Liu, and D. J. Fang (1984), Multifrequency study of ionospheric scintillation at Ascension Island, *Radio Sci.*, *19*(3), 695–706, doi:10.1029/RS019i003p00695.
Hasbi, A. M., M. A. M. Ali, and N. Misran (2007), Ionospheric TEC and scintillation during the 15–16 May 2005 major storm over equatorial anomaly region at ARAU, 2007 Asia-Pacific Conference on Applied Electromagnetics Proceedings, 1–5, Melaka, Malaysia.
Humphreys, T., M. Psiaki, A. Cerruti, and P. Kintner Jr. (2010), Data-driven testbed for evaluating GPS carrier tracking loops in ionospheric scintillation, *IEEE Trans. Aerosp. Electron. Syst.*, *46*(4), 1609–1623.
Hysell, D. L., and E. Kudeki (2004), Collisional shear instability in the equatorial *F* region ionosphere, *J. Geophys. Res.*, *109*, A11301, doi:10.1029/2004JA010636.
Hysell, D. L., M. C. Kelley, W. E. Swartz, and R. F. Woodman (1990), Seeding and layering of equatorial spread *F* by gravity waves, *J. Geophys. Res.*, *95*(A10), 17,253–17,260, doi:10.1029/JA095iA10p17253.
Jiao, Y. (2013), High latitude ionosphere scintillation characterization, MS thesis, Dep. of Electrical and Computer Engineering, Miami Univ. Oxford, Ohio.
Jiao, Y., Y. Morton, S. Taylor, and W. Pelgrum (2013a), High latitude ionosphere scintillation characterization, Proc. ION ITM, 579–584, San Diego, Calif.
Jiao, Y., Y. Morton, S. Taylor, and W. Pelgrum (2013b), On the correlation between ionospheric scintillation and geomagnetic field activities, Proc. ION GNSS+, 77–83, Nashville, Tenn.
Jiao, Y., Y. Morton, S. Taylor, and W. Pelgrum (2013c), Characterization of high latitude ionospheric scintillation of GPS signals, *Radio Sci.*, *48*, 698–708, doi:10.1002/2013RS005259.
Jiao, Y., Y. Morton, and S. Taylor (2014), Comparative studies of high-latitude and equatorial ionospheric scintillation characteristics of GPS signals, *PLANS 2014, 2014 IEEE/ION*, 37–42, doi:10.1109/PLANS.2014.6851355.
Kelley, M. C., M. F. Larsen, C. LaHoz, and J. P. McClure (1981), Gravity wave initiation of equatorial spread F: A case study, *J. Geophys. Res.*, *86*(A11), 9087–9100, doi:10.1029/JA086iA11p09087.
Kersley, L., S. Pryse, and N. Wheadon (1988), Amplitude and phase scintillation at high latitudes over northern Europe, *Radio Sci.*, *23*(3), 320–330, doi:10.1029/RS023i003p00320.
Kersley, L., C. Russell, and D. Rice (1995), Phase scintillation and irregularities in the northern polar ionosphere, *Radio Sci.*, *30*(3), 619–629, doi:10.1029/94RS03175.
Kintner, P. M., B. M. Ledvina, E. R. de Paula, and I. J. Kantor (2004), Size, shape, orientation, speed, and duration of GPS equatorial anomaly scintillations, *Radio Sci.*, *39*, RS2012, doi:10.1029/2003RS002878.
Kintner, P. M., B. M. Ledvina, and E. R. de Paula (2007), GPS and ionospheric scintillations, *Space Weather*, *5*, S09003, doi:10.1029/2006SW000260.
Li, G., B. Ning, B. Zhao, L. Liu, J. Y. Liu, and K. Yumoto (2008), Effects of geomagnetic storm on GPS ionospheric scintillations at Sanya, *J. Atmos. Sol. Terr. Phys.*, *70*(7), 1034–1045, doi:10.1016/j.jastp.2008.01.003.
Li, G., B. Ning, Z. Ren, and L. Hu (2010), Statistics of GPS ionospheric scintillation and irregularities over polar regions at solar minimum, *GPS Solut.*, *14*, 331–341, doi:10.1007/s10291-009-0156-x.
Liu, Z. (2011), A new automated cycle slip detection and repair method for a single dual-frequency GPS receiver, *J. Geod.*, *85*(3), 171–183, doi:10.1007/s00190-010-0426-y.
Liu, Z., R. Xu, Y. Morton, J. Xu, W. Pelgrum, W. Chen, and X. Ding (2013), A comparison of GNSS-based ionospheric scintillation observation in north and south Hong Kong, Proc. ION PNT, 694–705, Honolulu, Hawaii.
Mayaud, P. N. (1980), *Derivation, Meaning, and Use of Geomagnetic Indices*, *Geophys. Monogr.*, vol. 22, AGU, Washington, D. C.
Morton, Y., H. Bourne, M. Carroll, Y. Jiao, N. Kassabian, S. Taylor, J. Wang, D. Xu, and H. Yin (2014), Multi-constellation GNSS observations of equatorial ionospheric scintillation, Proc. URSI General Assembly & Sci. Sym., Beijing, China.
Morton, Y., Y. Jiao, and S. Taylor (2015), High-latitude and equatorial ionospheric scintillation based on an event-driven multi-GNSS data collection system, Proc. Ionospheric Effect Sym., Alexandria, Va.
Mushini, S., P. Jayachandran, R. Langley, J. MacDougall, and D. Pokhotelov (2011), Improved amplitude- and phase-scintillation indices derived from wavelet detrended high-latitude GPS data, *GPS Solut.*, doi:10.1007/s1029-011-0238-4.
Pelgrum, W., Y. Morton, F. van Graas, S. Gunawardena1, M. Bakich, D. Charney, S. Peng, J. Triplett, A. Vermuru, and P. Vikram (2011), Measurement and analysis of artificially-generated and natural ionosphere scintillations effects on GNSS signals, Proc. ION ITM, 950–958, San Diego, Calif.
Pi, X., A. J. Mannucci, U. J. Lindqwister, and C. M. Ho (1997), Monitoring of global ionospheric irregularities using the Worldwide GPS Network, *Geophys. Res. Lett.*, *24*(18), 2283–2286, doi:10.1029/97GL02273.
Prikryl, P., P. T. Jayachandran, S. C. Mushini, D. Pokhotelov, J. W. MacDougall, E. Donovan, E. Spanswick, and J.-P. St.-Maurice (2010), GPS TEC, scintillation and cycle slips observed at high latitudes during solar minimum, *Ann. Geophys.*, *28*, 1307–1316, doi:10.5194/angeo-28-1307-2010.
Prikryl, P., P. T. Jayachandran, S. C. Mushini, and R. Chadwick (2011), Climatology of GPS phase scintillation and HF radar backscatter for the high-latitude ionosphere under solar minimum conditions, *Ann. Geophys.*, *29*, 377–392, doi:10.5194/angeo-29-377-2011.
Redmon, R. J., D. Anderson, R. Caton, and T. Bullett (2010), A Forecasting Ionospheric Real-time Scintillation Tool (FIRST), *Space Weather*, *8*, S12003, doi:10.1029/2010SW000582.
Reggiani, N., O. C. Branquinho, T. A. Xastre, T. C. Nascimento, C. Dall'Orto, E. R. de Paula, I. J. Kantor, Mariangel Fedrizzi, and Luiz Felipe Campos de Rezende (2005), Influence of the geomagnetic activity on the GPS signal, *IEEE Xplore*, 125–128, doi:10.1109/IMOC.2005.1580097.

Rino, C. L. (1979a), A power law phase screen model for ionospheric scintillation: 1. Weak scatter, *Radio Sci.*, *14*(6), 1135–1145, doi:10.1029/RS014i006p01135.
Rino, C. L. (1979b), A power law phase screen model for ionospheric scintillation: 2. Strong scatter, *Radio Sci.*, *14*(6), 1147–1155, doi:10.1029/RS014i006p01147.
Rino, C. L., R. C. Livingston, R. T. Tsunoda, R. M. Robinson, J. F. Vickrey, C. Senior, M. D. Cousins, J. Owen, and J. A. Klobuchar (1983), Recent studies of the structure and morphology of auroral zone F region irregularities, *Radio Sci.*, *18*, 1167–1180, doi:10.1029/RS018i006p01167.
Rodrigues, F. S., M. Aquino, A. Dodson, T. Moore, and S. Waugh (2004), Statistical analysis of GPS ionospheric scintillation and short-time TEC variations over Northern Europe, *J. Inst. Navig.*, *51*(1), 59–75.
Rostoker, G. (1972), Geomagnetic indices, *Rev. Geophys.*, *10*(4), 935–950, doi:10.1029/RG010i004p00935.
Rumsey, D. J. (2011), *Statistics for Dummies*, 2nd ed., 384 pp., Wiley Inc., Hoboken, N. J.
Seo, J., T. Walter, E. Marks, T. Y. Chiou, and P. Enge (2007), Ionospheric scintillation effects on GPS receiver during solar minimum and maximum, *Proceedings of International Beacon Satellite Symposium 2007*, Boston, Mass.
Seo, J., T. Walter, T. Chiou, and P. Enge (2009), Characteristics of deep GPS signal fading due to ionospheric scintillation for aviation receiver design, *Radio Sci.*, *44*, doi:10.1029/2008RS004077.
Seo, J., T. Walter, and P. Enge (2011), Availability impact on GPS aviation due to strong ionospheric scintillation, *IEEE Trans. Aerosp. Electron. Syst.*, *47*(3), 1963–1973, doi:10.1109/TAES.2011.5937276.
Shang, S. P., J. K. Shi, P. M. Kintner, W. M. Zhen, X. G. Luo, S. Z. Wu, and G. J. Wang (2008), Response of Hainan GPS ionospheric scintillations to the different strong magnetic storm conditions, *Adv. Space Res.*, *41*(4), 579–586, doi:10.1016/j.asr.2007.05.020.
Skone, S. H. (2001), The impact of magnetic storms on GPS receiver performance, *J. Geod.*, *75*, 457–468, doi:10.1007/s001900100198.
Skone, S., K. Knudsen, and M. de Jong (2001), Limitations in GPS receiver tracking performance under ionospheric scintillation conditions, *Phys. Chem. Earth (A)*, *26*(6–8), 613–621, doi:10.1016/S1464-1895(01)00110-7.
Skone, S., F. Man, F. Ghafoori, and R. Tiwari (2008), Investigation of scintillation characteristics for high latitude phenomena, Proc. ION GNSS, 2425–2434, Savanna, Ga.
Smith, A. M., C. N. Mitchell, R. J. Watson, R. W. Meggs, P. M. Kintner, K. Kauristie, and F. Honary (2008), GPS scintillation in the high arctic associated with an auroral arc, *Space Weather*, *6*, S03D01, doi:10.1029/2007SW000349.
Taylor, S., Y. Morton, Y. Jiao, J. Triplett, and W. Pelgrum (2012), An improved ionosphere scintillation event detection and automatic trigger for GNSS data collection systems, Proc. ION ITM, 1563–1569, Newport Beach, Calif.
Taylor, S., Y. Morton, R. Marcus, H. Bourne, W. Pelgrum, and A. J. Van Dierendonck (2013), Ionospheric scintillation receivers performances based on high latitude experiments, Proc. ION Pacific PNT, 743–751, Honolulu, Hawaii.
Tsunoda, R. T. (1985), Control of the seasonal and longitudinal occurrence of equatorial scintillations by the longitudinal gradient in integrated E region Pedersen conductivity, *J. Geophys. Res.*, *90*(A1), 447–456, doi:10.1029/JA090iA01p00447.
Tsunoda, R. T. (1988), High-latitude F-region irregularities, a review and synthesis, *Rev. Geophys.*, *26*(4), 719–760, doi:10.1029/RG026i004p00719.
Valladares, C. E., R. Sheehan, M. P. Hagan, and E. MacKenzie (2002), Studies of ionospheric structures and their effects on systems, Air Force Research Lab. Report, AFRL-VS-TR-2002-1668.
Van Dierendonck, A. J., and B. Arbesser-Rastburg (2004), Measuring ionospheric scintillation in the equatorial region over Africa, including measurements from SBAS geostationary satellite signals, Proc. ION GNSS, Long Beach, Calif.
Van Dierendonck, A. J., J. A. Klobuchar, and Q. Hua (1993), Ionospheric scintillation monitoring using commercial single frequency C/A code receivers, Proc. ION ITM, Salt Lake City, Utah.
Van Dierendonck, A. J., Q. Hua, P. Fenton, and J. A. Klobuchar (1996), Commercial ionospheric scintillation monitoring receiver development and test results, Proc. ION Annual Meeting, 573–582.
Vikram, P. (2011), Event driven GPS data collection system for studying ionospheric scintillation, MS thesis, Dept. of Electrical and Comput. Eng., Miami Univ. Oxford, Ohio.
Xu, D., and Y. Morton (2015), GPS signal fading and carrier phase variations during strong equatorial ionospheric scintillation, Proc. ION ITM, Dana Point, Calif.
Xu, R., Z. Liu, M. Li, Y. Morton, and W. Chen (2012), An analysis of low-latitude ionospheric scintillation and its effects on precise point positioning, *J. Global Positioning Syst.*, *11*(1), 22–32, doi:10.5081/jgps.11.1.22.
Yeh, C. K., and C. H. Liu (1982), Radio wave scintillations in the ionosphere, *Proc. IEEE*, *70*(4), 324–360, doi:10.1109/PROC.1982.12313.
Yin, H., Y. Morton, M. Carroll, and E. Vinande (2014), Implementation and performance analysis of a multi-frequency GPS signal tracking algorithm, Proc. ION GNSS+, Tempa, Fla.